

CLOSING IN ON BACTERIORHODOPSIN: Progress in Understanding the Molecule

Ulrich Haupts, Jörg Tittor, and Dieter Oesterhelt

Max-Planck-Institut für Biochemie, D82152 Martinsried, Germany;

e-mail: tittor@biochem.mpg.de

KEY WORDS: retinal protein, membrane protein, proton translocation, proton pump

ABSTRACT

Bacteriorhodopsin is the best understood ion transport protein and has become a paradigm for membrane proteins in general and transporters in particular. Models up to 2.5 Å resolution of bacteriorhodopsin's structure have been published during the last three years and are basic for understanding its function. Thus one focus of this review is to summarize and to compare these models in detail. Another focus is to follow the protein through its catalytic cycle in summarizing more recent developments. We focus on literature published since 1995; a comprehensive series of reviews was published in 1995 (112).

CONTENTS

INTRODUCTION	368
GENERAL DESCRIPTION OF BACTERIORHODOPSIN FUNCTION	368
FOLDING AND RECONSTITUTION OF BACTERIORHODOPSIN	370
STRUCTURAL MODEL AND LIPID INTERACTIONS	373
CATION BINDING SITES IN BACTERIORHODOPSIN	377
THE CATALYTIC CYCLE	378
<i>Primary Reaction—The J Intermediate</i>	378
<i>K/KL Intermediates</i>	380
<i>The L Intermediate</i>	381
<i>M Intermediates</i>	382
<i>Completing the Cycle</i>	390

INTRODUCTION

Halophilic archaea thrive in high-temperature saturated salt brines that are exposed to bright sunlight. To extract energy as well as information provided by the light and its spectral composition, haloarchaea possess a set of four related retinal proteins in their cell membrane: bacteriorhodopsin (BR), halorhodopsin (HR), and two sensory rhodopsins (SRI and SRII).

Bacteriorhodopsin converts the energy of “green” light (500–650 nm) into an electrochemical proton gradient, which in turn is used for ATP production by ATP-synthases. Halorhodopsin is involved in maintaining iso-osmolarity of the cytoplasm during cell growth by transporting chloride ions into the cell, exploiting a similar spectral range (108). Sensory rhodopsin I and II, on the other hand, mediate phototactic behavior, thus permitting the cell to avoid harmful blue and UV light and to accumulate in regions favorable for photosynthesis (61, 146).

Bacteriorhodopsin is the focus of much interest and has become a paradigm for membrane proteins in general and transporters in particular. It also has technical applications not covered in this review. Instead, we focus first on refolding studies of BR *in vitro* as an example of membrane protein folding and then summarize insights obtained from recently published crystal structural models, including the role of lipids in determining biological properties. Finally, we follow the protein through its catalytic cycle, and evaluate the experimental data describing each step. We restrict ourselves to recent literature. Other recent reviews on BR and retinal proteins can be found in References 86, 109, and 112.

GENERAL DESCRIPTION OF BACTERIORHODOPSIN FUNCTION

As a basis for discussion, we start with a brief description of BR’s structural model and function. Although all retinal proteins fold into a seven-trans-membrane helix topology with short interconnecting loops, only BR naturally forms patches of two-dimensional crystals in the cell membrane, called purple membrane (PM). The helices (named A to G) are arranged in an arc-like structural model and tightly surround a retinal molecule that forms a Schiff base (SB) with a conserved lysine on helix G (K216 in BR). The cross section of BR with residues important for proton transfer is shown in Figure 1. Retinal separates a cytoplasmic (CP) from an extracellular (EC) half channel that is lined by amino acids crucial for efficient proton transport by BR (especially D96 in the cytoplasmic and D85 in the extracellular half channel). The geometry of the retinal, the protonation state of the Schiff base, and its precise electrostatic

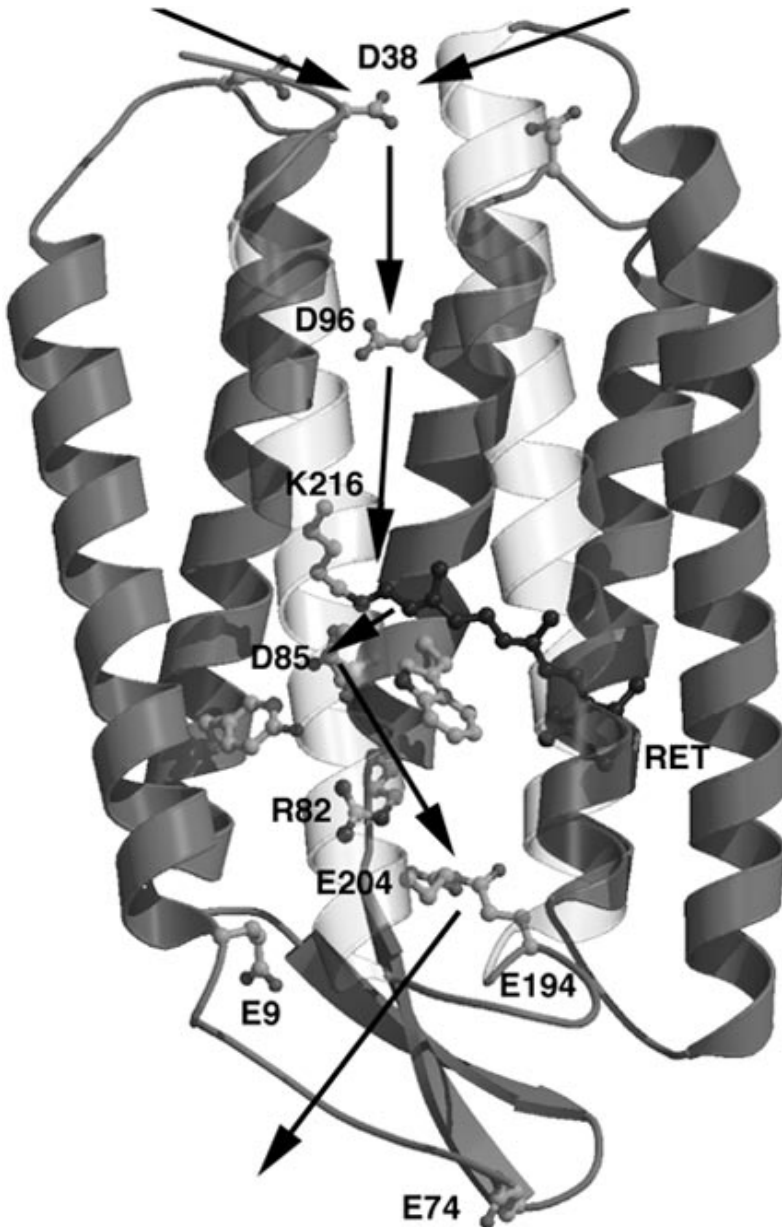


Figure 1 Cross section of the structural model VI (PDB entry BRR) of bacteriorhodopsin with selected residues important for proton transfer steps shown in *ball and stick* representation. The possible path of protons is indicated by *arrows*.

interaction with surrounding charges (D85, D212, and R82 in BR) and dipoles tune the absorption maximum to fit its biological function.

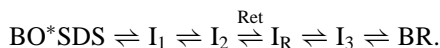
Absorption of a photon by BR initiates a catalytic cycle that leads to vectorial transport of a proton out of the cell. Thermal intermediates during the cycle were initially defined on the basis of time-resolved absorption spectroscopy and were termed J, K, KL, L, M₁, M₂, N, and O. Tremendous efforts have been made, using a host of biophysical methods, to determine the exact nature of changes in each step and to relate them to transport function. The cycle can be formally described in terms of six steps of isomerization, ion transport, and accessibility change (switch). Retinal first photo-isomerizes from an all-*trans* to a 13-*cis* configuration followed by a proton transfer from the Schiff base (SBH) to the proton acceptor D85. Concomitantly, a proton is released to the bulk phase by a group X, the exact nature of which is still under debate. To allow vectorial transport, the Schiff base needs to change its accessibility from extra-cellular to intracellular before reprotonation occurs from D96 in the cytoplasmic channel. After reprotonation of D96 from the CP surface, retinal re-isomerizes thermally and the accessibility of the Schiff base switches back to extracellular. These steps represent the minimal number of steps needed to account for vectorial transport in wild-type BR (WT-BR) and also for transport modes of its mutants (156a), halorhodopsin (5) and sensory rhodopsin (7, 49). These modes include inversion of direction of transport (156a), two-photon-driven transport, and the alternative transport of protons or chloride ions by one and the same molecule (132a, 155). Further information on BR and retinal proteins can be found in other recent reviews (81, 83–85, 87, 109).

FOLDING AND RECONSTITUTION OF BACTERIORHODOPSIN

Bacteriorhodopsin and its mutants or fusion proteins have been expressed in several heterologous systems (yeast: 60; *Xenopus leavis* oocytes: 104; COS-1 and Sf9 cells: 58) or even by cell-free translation (145). Translation products in *Escherichia coli* are not properly inserted into the membrane and had to be recovered from inclusion bodies and folded in vitro using a dimyristoyl phosphatidyl choline (DMPC) sodium dodecyl sulfate (SDS) mixed vesicle system (66, 90). This procedure formed the basis for recent studies on BR folding from a mechanistic point of view rather than for protein recovery. The folding kinetics of only two other membrane proteins have been studied so far, namely light-harvesting complex II from higher plants (11) and *E. coli* outer-membrane porin (151).

Folding of BR denatured in SDS was initiated by rapid mixing with detergent lipid micelles (SDS/DMPC/CHAPS) with or without retinal present, and the process was followed by time-resolved fluorescence (9, 10), absorbance (8, 12),

or circular dichroism (126). The simplest scheme emerging from these studies is described by



It should be kept in mind that BR in SDS still retains about 60% of its secondary structural model, equivalent to three or four transmembrane α -helices (90, 126). Complete loss of secondary structure can be induced by organic acids (66). Based on light-scattering changes, two kinetic components, ν_1 (250–420 s⁻¹) and ν_2 (2–10 s⁻¹), also observed as fluorescence changes, have been assigned to micelle mixing events; however, there are indications that ν_2 might also involve protein folding events to form intermediate I₁. Specifically, removal of the positive charge at position 175 (R or K), which is highly conserved among BR and HR sequences (101) and has been invoked in stabilizing helix arrangement (54), results in the loss of ν_2 (8). CD spectroscopy suggests the formation of a helical structure during the folding process corresponding to about 70 amino acids. The foldings of 40 amino acids are not time-resolved (126). The remaining 30 amino acids adopt an α -helical conformation in the rate-limiting step ($\nu_3 = 0.01 \text{ s}^{-1}$) leading to intermediate I₂. This step depends on the rigidity/composition of the bilayer (12). I₂ is the key intermediate, with native-like helical content and a well-structured retinal binding pocket. Addition of retinal to pre-equilibrated I₂ results in formation of intermediate I_R in a second-order reaction. I_R is characterized by an absorption maximum of 430 nm and most likely has retinal bound in its pocket but without the Schiff base formed. It would then correspond to the intermediate absorbing at 430/460 nm found when bleached PM is reconstituted with retinal (137) or to the final chromophore in K216 mutants unable to form a covalent linkage with retinal (141). The final phase of folding involves formation of the Schiff base and small structural rearrangements of the helices with at least one intermediate (time scale of minutes). Most of the apoprotein (bacterioopsin, BO) folding is suggested to occur up to intermediate I₂, when retinal slips into a preformed binding pocket. In this context, an interesting observation is that the pK_a of the Schiff base of BR depends on preparation conditions (79). Addition of retinal to a culture of JW5 cells, which are deficient in retinal synthesis, leads to *in vivo* BR formation with a Schiff base pK_a > 10.2, as in WT-BR. BR reconstituted *in vitro* from apomembranes (AM) of JW5 cells and retinal had a pK_a of 8.5. The authors suggest that during *in vivo* folding, retinal acts as a template for the exact folding of the polypeptide chain, leading to a tighter packing of the side chains around the chromophore. Despite these differences in the Schiff base pK_a, the photocycle kinetics of M-rise and decay are very similar. One difference in the preparation conditions seems to be that biogenesis of BR is under high salt, whereas reconstitution as well as in

vitro folding studies are performed in low salt. Although BR is stable under all conditions, a folding process to achieve the final structural model might be affected by ionic strength.

Folding of functional BR is possible from two or three fragments containing complementary sets of helices (70, 95, 113). These studies demonstrate that none of the loops connecting helices A through F is essential for correct association and orientation of the helices, although they stabilize the structure (71, 95). Even fragments containing redundant sets of helices (e.g. A–E and C–G) form functional BR (95). It has also been suggested that the helices (or sets of helices) represent independent folding units that are preformed before the functional molecule is assembled in a second stage of folding (122). This may not be true for each of the helices; it was found that peptides corresponding to helices A to E form stable transmembrane α -helices but that helix F does not form any stable secondary structural model at all, helix G forms a hyperstable β -sheet, and helix C reversibly inserts into the membrane in a pH-dependent manner (67, 68). For these peptides, some external constraints may be necessary to adopt a helical structure.

BR may also be reconstituted from BO and inactive retinal, e.g. 9-*cis* retinal can be used as a “caged retinal.” 9-*cis* retinal is fixed in the binding pocket of BO but does not form a Schiff-base linkage (138). Upon illumination with blue light, retinal isomerizes to all-*trans* and reconstitutes the chromophore (34, 93). This approach was used to study the role of water during reconstitution (127, 128). Films of the BO/9-*cis* complex (BR₃₉₀) were equilibrated to different humidity and irradiated with blue light. Low humidity leads to formation of a species absorbing at 470 nm that has no covalent linkage to K216, whereas high humidity favors a 570-nm-absorbing species. Exposing BR₄₇₀ to water vapor converts BR₄₇₀ and residual BR₃₉₀ to BR₅₇₀, demonstrating the role of water in the formation of the Schiff-base linkage. Two forms of the 570-nm-absorbing species could be differentiated. Above 86% humidity, WT-BR₅₇₀ is formed, whereas below 86%, a species called BR'₅₇₀ can be distinguished by the rise and decay kinetics of its M' intermediate and the absorbance shifts observed upon desiccation. In contrast to the mutant D96N, which forms a mixture of BR₄₇₀ and BR'₅₇₀ even at 100% humidity, the mutant E204Q converts to BR₅₇₀ at humidities as low as 57%. It was suggested that these two residues have key roles in binding water molecules inside the protein.

In an attempt to identify groups that protonate/deprotonate during reconstitution (33), the BO/9 *cis*-to-BR₅₇₀ reaction was followed with Fourier-transform infrared difference spectroscopy using WT-BR and mutants D38N, D96N, D115N, and E204Q (131). Surprisingly, none of the aspartate residues undergoes a protonation change; only changes in the hydrophobicity of the environment are seen. Instead, a hydrogen-bonded network including the side

chains of E204, D85, R82, Y57, and bound water was suggested to be responsible for proton release/uptake during chromophore reconstitution.

STRUCTURAL MODEL AND LIPID INTERACTIONS

Although the three-dimensional structural model of a protein determined with classical X-ray crystallography or electron diffraction is static, it is invaluable in understanding the function of a protein because it guides the interpretation of dynamic changes observed in time-resolved measurements or the design of mutants thought to be of functional significance. The unique two-dimensional crystalline nature of PM allowed determination of the molecular structural model with electron diffraction methods at cryo temperatures. The initial low-resolution model of PM (54; 1BRD: structural model I) was later refined to a resolution of 3.5 Å (43; 2BRD: structural model II) and 3.0 Å (77; 1AT9: structural model III). Data were taken from either completely dried samples in the presence of glucose (I, II) or partially dried samples in the presence of trehalose (III), respectively. Three recent X-ray crystallographic studies [117, 1AP9: structural model IV; 92, 1BRX (V); 32, 1BRR (VI)] seem to add even more information on the precise location of amino acid side chains, internal water molecules, and lipids as well as their interaction with the protein. BR crystals were obtained from the lipid cubic phase (IV, V) or were grown on benzamidine crystals from detergent phase (VI). In all cases, data collection was done at cryo temperatures. It should be pointed out, however, that the X-ray crystallographic studies do not provide independent verification of the two electron crystallographic structural models because they used the coordinates of structural models II and/or III during the molecular replacement procedure. The quality of the derived models, however, strongly depends on the search model used and whether simulated annealing and omit maps were correctly calculated to minimize model bias. Table 1 provides some key distances discussed in the respective publications and below. Obviously, some distances deviate from each other by larger values than the reported resolution would allow. This indicates that either the models are not yet completely correct or that the different conditions of sample preparation, e.g. native membrane versus detergent or lipid phase, cause differences in the structures. Both causes may contribute to the deviations.

All structural models agree on the general arrangement and orientation of the helices. Concerning proton transport, the most interesting parts of the structural models are the proton release pathway on the extracellular side (SBH, D85, D212, R82, E194, E204, E9, T205, T89, Y83, Y57, Y185, W86, water), the reprotonation pathway in the cytoplasmic half channel (D96, T49, D38, water), and the cytoplasmic membrane surface for proton capture and guidance (D104,

Table 1 Distance comparison between the different structural models for residues in bacteriorhodopsin important for proton transfer and conformational rearrangements. Distances are given in Å. Given a favorable orientation, hydrogen bonds are considered possible in the distance range of 2.5 Å to 3.5 Å.

Distance between		PDB-entry code				
Atom A	Atom B	AP9/IV	AT9/III	BRD/II	BRX/V	BRR(B)/VI
K216NZ	D85OD2	4.31	3.85	3.71	4.19	4.34
	D85OD1	6.22	4.31	3.82	4.28	4.81
	D212OD1	5.52	3.15	3.96	3.66	3.59
	D212OD2	4.43	3.53	4.81	4.87	4.81
	T89OG1	3.57	3.71	3.81	3.99	4.78
D212OD1	W86NE1	4.53	3.64	2.86	3.74	3.60
D212OD2	W86NE1	3.49	4.74	3.41	4.27	3.97
D212OD2	Y57OH	2.82	1.98	2.87	2.80	2.67
D212OD1	Y185OH	2.89	2.94	2.88	2.56	2.6
D212OD2	Y185OH	4.30	5.09	4.96	4.61	4.61
D212OD2	R82NH1	6.21	5.32	6.38	3.34	4.34
	R82NH2	8.45	5.43	8.29	4.34	6.52
D85OD1	T89OG1	5.92	4.38	3.10	2.73	4.82
D85OD2	T89OG1	3.94	4.12	4.90	4.55	2.96
D85OD1	W86NE1	4.39	4.53	5.50	5.12	5.26
D85OD2	W86NE1	4.36	6.42	4.29	4.28	4.89
W86NE1	R82NH1	6.42	4.71	7.10	4.37	6.09
	R82NH2	8.63	4.33	8.82	6.56	8.16
	Y83OH	8.60	8.51	8.64	8.16	8.47
E194OE1	E204OE1	10.71	9.00	6.93	5.41	5.28
	E204OE2	10.54	7.83	8.40	3.93	3.76
E194OE2	E204OE1	9.72	7.35	7.73	4.52	4.01
	E204OE2	9.98	6.09	9.45	4.00	3.45
E194OE1	Y83OH	4.94	8.82	6.60	2.83	2.67
E194OE2	Y83OH	3.39	8.51	5.53	4.80	4.01
E204OE1	Y83OH	9.43	5.81	7.88	8.13	7.48
E204OE2	Y83OH	10.14	6.08	10.05	6.35	6.05
E204OE1	R82NE	7.99	3.45	4.87	7.17	4.84
E204OE2	R82NE	9.37	4.54	6.41	5.72	5.47
E204OE1	R82NH2	7.38	4.39	3.02	7.71	4.75
E204OE2	R82NH2	8.79	6.08	4.19	6.55	6.14
D96OD1	T46OG1	4.00	5.61	5.91	3.93	2.45
D96OD2	T46OG1	3.32	4.48	5.04	3.64	3.61
	K216NZ	11.01	10.95	13.76	11.17	13.30
	D38OD1	12.79	15.65	10.55	13.15	9.93
	E166OE2	12.24	17.63	17.79	—	16.47
Retinal		twisted	straight	straight	straight	twisted
RetC20	RetC19	5.93	5.45	5.45	5.39	5.44
RetC19	RetC18	4.83	5.26	5.26	5.11	5.21

D102, D36, lipid head groups). Several cavities large enough to accommodate one or more water molecules have been identified in each structural model. The highest resolution, allowing localization of water molecules, is needed to differentiate mechanisms of proton transport based on the identification of hydrogen bonds. The role of water molecules in the transport mechanism, although suggested long ago (59), found increased appreciation lately, but their positions mostly eluded exact identification in the structural models. Only in structural model V are three water molecules localized on the basis of their electron density; otherwise their presence is inferred from the identification of cavities large enough to accommodate them. The presence of 7–12 water molecules in the EC and CP channel was detected by neutron diffraction data; four of these molecules are tightly bound in the structure (114).

The distance between the protonated Schiff base (SBH) and D85 (4.2 Å to OD2 in structural model VI) is too far for a direct hydrogen bond. Although in structural model IV no water molecules are found in hydrogen-bonding distance to D85, in structural models V and VI a cavity large enough to accommodate water molecules between SBH, D85, and R82 is identified. The oxygen atom OD2 of D85 is hydrogen bonded to T89 (not in III and IV) and the two oxygen atoms OD1 and OD2 of D212 to Y57 and Y185, respectively. Additional hydrogen bonds are found between OD1 of D212 and the SBH (II, III) whereas OD2 forms a hydrogen bond to W86 in model II but to R82 and the water between the SBH and D85 in model V. The orientation of R82 has been much debated, as it points downwards in structural model II, although it was expected to be part of the complex counter ion of the Schiff base (6). In more recent structural models (III, V, VI), R82 points toward D212, to which a hydrogen bond is postulated (V) or appears to be immersed in a local water pool of two surrounding cavities large enough to accommodate several water molecules (V, VI). The following alternative proton-release pathways are discussed. The orientations and distances of the amino acid side chains slightly favor a release through D85, R82, T205, and E9 in structural models II and IV, whereas the alternative involves D85, R82, E204, and E194 (V, VI), the latter two forming a dyad in the proton-release pathway (VI). Despite the detailed mechanisms proposed, it should be kept in mind that mutational analysis bears problems if used to draw conclusions about wild-type proton transfer pathways. Removal of a component in the proton exit pathway possibly opens alternatives that do not contribute to proton transport in the wild type. One such example is the reprotonation kinetics of wild-type, D96N, and D96G mutants (99).

The reprotonation of the Schiff base occurs from D96 over a distance of ~12 Å. No obvious proton pathway is discernible between D96 and the Schiff base in the dark state of the protein. A cavity capable of holding one or two water molecules is located near D96 (II, V, VI) and may be part of the reprotonation pathway after the Schiff base has changed its accessibility during

the cycle. The existence of hydrogen-bonded networks in the extracellular and cytoplasmic half channel were suggested on the basis of continuum bands found in FTIR studies (88, 124). Also, azide was suggested to accelerate M-decay in the D96N mutant by inducing a hydrogen-bonded network in the cytoplasmic half channel (88). D96, in turn, is reprotonated from the cytoplasmic membrane surface, which functions as a proton collector (20, 102). The reprotonation pathway of D96, by all likelihood starting at D38, again has no obvious H-bond network spanning the 12 Å distance in the initial state structural models. Residue D38 was identified to play a key role in the reprotonation of D96 as well as in the structural changes associated with the $M_1 \rightarrow M_2$ transition (135). The cytoplasmic surface carries an excess of negatively charged groups, i.e. acidic residues in loops (D36, D102, D104, E161, E166) and the C terminus (E227, E234, E237, D242) as well as negatively charged phospho head groups of surrounding lipids. These protonatable groups are potentially involved in proton capture from the bulk and allow rapid proton diffusion along the membrane surface (53).

The purple membrane contains up to 10 lipid molecules per BR monomer, which account for 25% of its mass. In *Halobacterium salinarium*, C2 and C3 of sn-glycerol is ether linked to dihydrophytanoyl side chains (archeol), whereas C1 carries one of several polar head groups to form phosphatidylglycerol phosphate (PGP), phosphatidylglycerol phosphate methylester (PGP-Me), phosphatidylglycerol sulfate (PGS), and a sulfated triglycoside lipid (S-TGA-1). Partial removal of lipids by mild detergent treatment affects photocycle kinetics (29). Wild-type kinetics can be restored by adding back halobacterial lipids, whereas phospholipids lacking the ether-linked dihydrophytanoyl side chains are not effective (100, 121), suggesting a specific role for the lipids in maintaining BR functionality.

The structural model II includes ten lipid molecules per BR monomer; however, half of the dihydrophytanoyl side chains and all of the head groups are disordered. Two lipid molecules showed electron density in structural model VI, i.e. one S-TGA-1 and the side chains of one phospholipid molecule. The latter bind tightly to the protein because they are not fully removed even in detergent-solubilized BR (116); they seem to play a special role in stabilizing the PM structure. Specific labeling of S-TGA-1 with deuterated sugars allowed the localization of two molecules per BR monomer in a neutron diffraction-study (166).

Three S-TGA-1 molecules are located within the BR trimers (corresponding to side chains 261 in model II). One of their elongated 3-phytanoyl chains specifically fits into a hydrophobic groove on helix D, providing a molecular explanation for the finding that mutations on helix D disrupt PM formation (82). The second phytanoyl chain makes tight contact with W80 on helix C

and might provide part of the driving force for trimer formation. As expected, substituting W80 with smaller residues disrupts PM formation (H Besir & D Oesterhelt, unpublished), presumably by destabilizing the trimer units. The second S-TGA-1 molecule mediates interaction between trimers by contacting helices A/G and helix E of two monomers (166). Residues W12 and W10 on helix A are likely candidates for interactions with the lipid, and preliminary results show decreased PM formation upon mutation of W12 (H Besir & D Oesterhelt, unpublished).

An electron-crystallographic structural model of deoxycholate-treated PM (42), which lacks roughly half of the lipid molecules, reveals virtually identical structural features of the protein monomer, whereas electron density at positions corresponding to the second S-TGA-1 molecule between trimers is missing. As a result, the arrangement of the trimers is changed and leads to different contacts.

Although the structural information gained from X-ray diffraction studies is static, the temperature factors give an indication of the flexibility of different parts of the molecule. Roughly, the temperature factors increase from the center of the structural model embedded in the membrane toward the loop regions on either side of the membrane. Direct experimental evidence for a hard core vs a soft shell was obtained from neutron diffraction studies of selectively labeled BR (125). Obviously, the amplitude of thermal fluctuations around retinal must be smaller than the structural changes induced by retinal isomerization. On the other hand, the outer parts of the molecule must be flexible enough to allow for larger changes that might be necessary for proton transport. Upon dehydration and delipidation of PM, a reduction of internal flexibility was found that points toward a role of the lipids in influencing protein dynamics (35).

CATION BINDING SITES IN BACTERIORHODOPSIN

Deionization of purple membranes leads to a color change from purple to blue that is reversed upon addition of mono-, di- or trivalent cations. Five (76) to sixteen (69) cation binding sites of high as well as low affinity were reported. Enzymatic removal of the carboxy terminus of BR eliminates all but one binding site of the low-affinity type, indicating their surface location. Based on the finding that replacement of D85 or D212 reduces the binding constant of the high-affinity site while leaving the low-affinity binding unaffected (172), it was suggested that the former is composed of the protonated Schiff base, D85, D212 and R82. Thus the change in electrostatics in the immediate vicinity of the retinal causes the color change from blue to purple (69, 115, 143). However, none of the published BR structural models gives any indication for the presence of a cation, nor did any of the molecular dynamic calculations include

a cation close to the Schiff base in order to yield reasonable pK_a values for the protonatable groups in BR (6, 107, 132).

In an alternative model, the metal ions were treated as free cations uniformly distributed on the surface of PM, thereby influencing the surface pH via the Gouy-Chapman effect (152). A low surface pH in the absence of cations would lead to protonation of intrinsic carboxylates, i.e. D85 and D212, which has been shown to induce a redshift of the absorption maximum. Strong experimental evidence for this model comes from the finding that the kinetics of the blue-to-purple transition is independent of the size and charge of the cations, such as monovalent or divalent ammonium ions up to the size of $\sim 10 \text{ \AA}$ (37). In quantum chemical calculations, small organic cations could be accommodated in the retinal binding pocket but not at the site proposed for Ca^{2+} binding (153) and not of the size used in the experiments described above. These cations could not be accommodated, by any means, in the retinal binding pocket nor in any other location in the interior of BR (3). Thus, a model based on D85, D212, and R82 as the cation binding site seems unlikely, and further experimentation is needed to clarify which surface groups are involved in low- and high-affinity cation binding.

THE CATALYTIC CYCLE

Primary Reaction—The J Intermediate

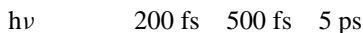
The photoreaction in bacteriorhodopsin leading from all-*trans* to 13-*cis* retinal is far more selective and efficient than photoreactions of retinal in solution. Thus, much attention has been paid to understanding this reaction in the protein, and a variety of spectroscopic experiments have been carried out to elucidate the primary events in BR. Due to improvements in laser and detector technology, the time resolution was increased to a few femtoseconds; the results of recent experiments are discussed in this section. The detailed knowledge of electronic and nuclear dynamics of the photoisomerization of retinal in bacteriorhodopsin will likely increase understanding of the efficiency and selectivity of the observed reaction and may provide a tool for developing technical devices that convert light energy into chemical energy.

Electrons of the uniformly light-adapted initial state are excited by photons of the appropriate wavelength to the Franck-Condon region of the excited-state surface of S_1 . The wave packet develops for some time on the excited-state surface(s) and then returns to the ground state, S_0 . The quantum efficiency for isomerization is 0.64 (156); therefore, 36% of the molecules return to the initial state. Questions about the primary reaction of BR concern the shape of the potential energy surface, involvement of S_2 , and the crossing point to S_0 .

Two different models for the primary reaction exist, and for each, supporting as well as contradicting experimental evidence was obtained. One is the two-state model with an electronic ground state and one excited state, which was

introduced first and is therefore called the conventional model. The other is the three-state model, which includes a second electronic excited state.

The two-state model is represented by a sequential and barrierless reaction scheme on the S_1 potential surface in the form



Here J_{625} represents a thermal intermediate in the electronic ground state S_0 . Experiments in the wavelength range from 600 to 900 nm reported decay times for stimulated emission measured at about 200 and 500 fs and set the lower limit for the excited-state decay (26, 96). The 200-fs component was interpreted as the development of the wave-packet from the Franck-Condon state downhill by about 2800 cm^{-1} to the minimum in the excited-state potential curve along the isomerization coordinate.

Fluorescence upconversion measurements revealed time constants of 90 to 240 fs and 600 to 900 fs for the fluorescence decay at wavelengths ranging from 680 to 900 nm and an additional third one of 9 to 13 ps that is not seen in stimulated emission (31). The occurrence of this third component in the fluorescence decay questions the one-dimensional potential surface model above and could indicate branching in the excited state. Excited-state absorbance with maxima around 480 nm (26, 120) and 760 nm (47) was found in transient absorption measurements and could interfere with stimulated emission.

Anti-Stokes Raman scattering reveals a decay time of 2.5 ps of the ethylenic stretch intensity of the chromophore (13, 27). This type of Raman scattering can be observed only from vibrationally excited molecules and argues for J being the vibrationally hot K intermediate. However, the difficulty in distinguishing in this type of experiment between the vibrationally excited BR ground state (36% after deexcitation) and the vibrationally excited photoproduct weakens the argument.

From more recent time-resolved absorbance measurements, a three-state model for the reaction sequence was proposed (38, 47). These authors attributed the positive absorbance change at $\sim 700 \text{ nm}$ to the residual difference between the excited-state absorbance band ranging from 600 nm up to 900 nm and the stimulated emission band observed in the same wavelength range. Thus, the hot ground-state intermediate, J, of the conventional model appears in the three-state model as an excited-state phenomenon. Because both the excited-state absorption band and the stimulated emission band can not be measured separately but have to be calculated from the difference spectrum, the nature of J remains unknown. A stronger argument against the conventional model is based on the following experimental facts. Two independent studies show that the stimulated emission spectrum does not change from 50 fs to about 1 ps,

indicating a small barrier on the S_1 surface incompatible with the conventional model (46, 47) and implying a temperature dependence of the decay time. However, excited-state decay was found to be temperature independent down to 4° K (89). The barrier is assumed to arise from an avoided crossing region of the S_1 and S_2 states. During this time the twist around the $C_{13}=C_{14}$ bond should be near zero. Crossing the small barrier leads to fast progress in the isomerization process and population of the first 13-*cis* intermediate K. In this model the transition from the first, nonreactive part of the excited-state surface to the reactive part of S_1 with a steep slope along the isomerization coordinate occurs in 500 fs and then retinal twists and is directed by the protein into a second avoided crossing region between S_1 and S_0 to reach the 13-*cis* ground state, K. The protein is assumed to control the quantum yield, but retinal provides the driving force for isomerization. This model explains differently from the conventional model why it is not possible to trap the J intermediate even at 4° K, but it cannot account for the anti-Stokes Raman scattering results if they are not attributable to hot ground-state BR.

Additional important information about the primary reaction comes from experiments with BR containing locked retinal to prevent isomerization around the $C_{13}=C_{14}$ bond. A 200-fs decay constant for excited-state dynamics was determined independent of temperature (78° K to 273° K) by determining the time correlation function of absorption spectra (1). In experiments with picosecond time resolution, an intermediate was found (called T5.12) with properties similar to those of J_{625} (22). If T5.12 is identical to J_{625} , then isomerization around $C_{13}=C_{14}$ is not a prerequisite for producing the absorbance change; it might be that it represents excited-state absorbance (38, 47). Atomic force microscopy could detect a presumed change in the absence of retinal isomerization (130). Surprisingly, this conformational change lasts long enough to allow light-enhanced reduction of the Schiff base by hydroxylamine (129). This would be in accordance with molecular dynamics calculations showing that the polarization change in the excited state of retinal could trigger a protein dielectric polarization relaxation (168). Although this relaxation was calculated to occur on the ps time scale, it could lead to a conformational change of the protein, which might persist even after the chromophore has returned to the S_0 state. Such a phenomenon was found for the primary photoreaction of photoactive yellow protein where a nonisomerizable chromophore triggers a complete photocycle (21).

To summarize the current understanding of the primary events in the primary reaction of bacteriorhodopsin, both models are neither unequivocally disproved nor proved, and more experimental work is needed.

K/KL Intermediates

It is generally accepted that the K intermediate rises within a few picoseconds. Assuming that the intermediate following K is L, which rises in 1 μ s,

following excitation implies that the lifetime of K is about 6 orders of magnitude greater than prior intermediates and therefore is the relatively longest-lived intermediate.

An SVD analysis (134) of time-resolved FTIR data showed a marked difference between FTIR spectra taken at 10 ns and 1000 ns, especially at the hydrogen out-of-plane modes at 958 cm^{-1} and 985 cm^{-1} ; these spectra were assigned to the KL intermediate described earlier (142). The HOOP mode at 985 cm^{-1} is not detected if BR is illuminated at 77° K but is detected if illuminated at 135° K . The band at 985 cm^{-1} was assigned to the C_{15} HOOP and can be taken as a band indicative for KL (165). A similar conclusion was reached by an independent study (44). On the other hand, the change in the ethylenic stretch region expected to accompany the shift in absorption maximum (4) could not be found. In accordance with these results, an earlier transient absorbance study (98) determined a change in the difference spectra between 50 ns and $3\ \mu\text{s}$ with a clear isosbestic point and an activation barrier for that transition.

Keeping the many degrees of freedom in mind that are described by only a single reaction coordinate, it is not surprising that the $\text{K} \rightarrow \text{KL}$ transition is silent with respect to some spectroscopic features (within the applied resolution, e.g. $\text{C}=\text{C}$ stretch frequency), whereas it shows up in others (λ_{max}). A similar phenomenon applies to the different M-species discussed below. In summary, it seems justified to regard KL as an intermediate, i.e. it represents a local energy minimum along the reaction coordinate.

The L Intermediate

The KL-to-L transition has been studied by step-scan FTIR spectroscopy (44). The temporal behavior at different wavelengths could be fitted with a single exponential in each case. However, two groups of bands appeared that are characteristic for changes in the vicinity of the β -ionone ring or the Schiff base and develop with time constants of 400 ns and $2\ \mu\text{s}$, respectively. It was concluded that the structural relaxations during the KL-to-L transition proceed with different kinetics, e.g. a fast change near the β -ionone ring followed by a slow change at the SB.

In the L intermediate, the stage must be set for the subsequent proton transfer from the SBH to D85 in the L-to-M transition. This implies a strong interaction between D85 and SBH in L. Indeed, in a NMR study (65) it was found that the interaction between the SBH and its counterion is much stronger in L than in either N or BR. The chemical shift value of the SB nitrogen argued for double-bond strain, in particular around the $\text{C}=\text{N}$ bond. Also, it was concluded that the chromophore is not in a 13,14-*dicis* configuration, as invoked in some models of the catalytic cycle (39, 140). Based on a series of FTIR studies (74, 169–171), a very detailed picture of hydrogen bonding between water molecules, peptide carbonyls, and side chains in the L intermediate was suggested (94). Briefly,

a water molecule that is bound to the SBH and D85 in the initial state forms stronger hydrogen bonds to both these groups in the L intermediate, and in addition, a further hydrogen bond is established to D212 that is necessary for proton transfer (74). These changes near D85 are suggested to be transmitted to D96 in the CP channel through an H-bonding interaction involving water molecules, T46, the C=O of V49, and D96 (169, 171). Trp182 interacts with the 9-methyl group of retinal, thereby affecting the equilibrium between M and L, and its substitution in the W182F mutant slows M formation (170).

Since no global structural changes were detected in an electron diffraction study of the L intermediate (55), the signals detected by FTIR spectroscopy represent relatively small local perturbations, yet these lead to a decrease of the pK_a of the SBH (16, 41) and an increase of the pK_a of D85 (14, 127) to allow the proton transfer in the L-to-M transition. Concomitant to this transition, a proton that appears at the extracellular surface (2, 52) must be released by an entity other than D85, named XH. Amino acid side chains R₈₂, E₂₀₄, E₁₉₄, or a hydrogen-bonded network including these and water molecules, have been suggested (92, 124).

M Intermediates

To allow vectorial proton transport, de- and reprotonation of the Schiff base must occur from different sides of the membrane. Therefore, at least two M intermediates must exist that differ in the accessibility of the Schiff base and are interconverted in a step called the "switch," i.e. $M_{ec} \rightarrow M_{cp}$, where ec and cp indicate extracellular and cytoplasmic accessibility, respectively. In addition, the switch should increase the Schiff base pK_a to make it a proton acceptor. The exact nature of changes that represent the switch has eluded experimental identification. Two extremes can be envisioned as to what molecular changes represent the switch. On the one hand, the switch could be induced by small changes in the chromophore retinal, such as a single bond rotation from a 13*cis*-14*cis* to a 13*cis*-14*trans* configuration (140). The other extreme attributes the switch completely to conformational transitions of the protein moiety changing from a T- to a C-geometry that can accommodate the all-*trans* and 13-*cis* retinal, respectively (36). Most likely, the actual mechanism involves both components. Regarding the identification of two M substates, there is no clear experimental evidence whether intermediates designated M₁ and M₂ throughout the literature are identical to M_{ec} and M_{cp}. Even worse, due to the different experimental conditions, it is unlikely that the same M species have been described in the different studies. For example, the different M states have been stabilized by low temperature (110), the use of mutants D96N (18) or D96G (149), or incubation with arginine or guanidine hydrochloride at high pH (24, 106), osmotically active substances like sucrose and glycerol (19), or by dehydration (80).

In time-resolved absorption studies, it has long been recognized that the M intermediate rises and decays with more than one time constant, giving indirect kinetic evidence for the existence of several M species (see 87). In a series of studies, Varo & Lanyi introduced a linear photocycle model ($K \leftrightarrow L \leftrightarrow M_1 \rightarrow M_2 \leftrightarrow N \leftrightarrow O \rightarrow BR$) including an irreversible $M_1 \rightarrow M_2$ step that was required to model the kinetic data (158–160). Similar results were obtained from an analysis of resonance Raman data (3, 105). From the enthalpy and entropy changes of this transition, it was concluded that it is associated with major conformational changes that could thus provide the switch (159). The specific deceleration of the $M_1 \rightarrow M_2$ transition found at lower relative humidities (161) or in the presence of osmotically active substances (19) points to a crucial role of water in changes associated with M. Whereas M_1 and M_2 absorb maximally at 411 nm in the case of WT-BR, a blueshift to 404 nm of the M_2 absorption maximum in the case of mutant D96N (173) and a redshift of 4 nm for the M_1 state of solubilized BR (158) were detected.

Fourier-transform difference spectroscopy is very sensitive to conformational changes of proteins, which show up as spectral features in the amide I ($1650 \pm 30 \text{ cm}^{-1}$) and amide II ($1550 \pm 30 \text{ cm}^{-1}$) regions. FTIR has been used to study M species trapped at 240–260° K (110). The M species at 240° K was characterized by a strong positive band at 1762 cm^{-1} , representing protonated D85 and negative bands in the amide I region (1670 cm^{-1} , 1660 cm^{-1} , 1650 cm^{-1}). Specifically, the ratio of $1670 \text{ cm}^{-1}/1660 \text{ cm}^{-1}$ was < 1 , and absorption at 1550 cm^{-1} was slightly negative. The positive, broad amide II band was located at 1564 cm^{-1} and displayed a shoulder at higher wave numbers. In contrast, the M species at 260° K showed a band at 1755 cm^{-1} for D85 and the ratio of $1670 \text{ cm}^{-1}/1660 \text{ cm}^{-1}$ was > 1 ; at 1650 cm^{-1} , a strong positive band appeared, and the amide II band was more narrow and shifted to 1556 cm^{-1} . These differences were interpreted to be indicative for M_1 and M_2 , respectively. However, this assignment was later revised (111) on the basis of experiments supposedly yielding pure M/BR difference spectra. After trapping M at different temperatures, blue light was used to selectively drive back the M intermediate to the initial state. The resulting spectra at 220° K and 270° K were found to be virtually identical and similar to the M spectrum at 240° K in previous work (111). Differences seen before at 260° K were attributed to the presence of some N intermediate, an interpretation that was in turn questioned (135; see below).

The mutant D96N conveniently allows M accumulation due to the drastically slowed M-decay at high pH values (18, 62, 157). The resulting FTIR difference spectrum at 274° K was suggested to be composed of contributions of two species. M, for which a pure spectrum could be recorded at 230° K (similar to M_1 ; 110, 119), and a species defined as M_N , which displayed features in the amide I region typically found for the N intermediate, whereas

the chromophore bands suggested a deprotonated Schiff base (133). The most significant differences to the M spectrum recorded at 230° K were the shifted D85 band at 1755 cm⁻¹, a strong negative band at 1670 with only a shoulder at 1660 cm⁻¹, a strong positive band at 1650 cm⁻¹, and a narrow amide II band at 1557 cm⁻¹. Thus, in M_N the protein has already adopted the conformation of the N state but proton transfer to the Schiff base has not yet occurred. This intermediate might be undetectable in the catalytic cycle of wild-type (WT) BR.

Low temperature was also used to stabilize M states in glucose-embedded WT-BR at 81% relative humidity (r.h.) (119). Species trapped at 204° K and 260° K were designated M₁ and M₂, respectively, and could be distinguished by the same features pointed out before (110), although visible spectra suggested no significant contributions of intermediates other than M (118), in contrast to results of earlier work (110, 111). To resolve this discrepancy, the blue-light reversal experiment (111) was repeated with glucose-embedded samples (164). At 240° K trapping temperature, the difference spectrum was similar to the ones obtained before (110, 111, 119) and designated M (probably equivalent to M₂). The spectrum at 260° K, on the other hand, displayed N-typical features and was interpreted to represent a mixture of M and M_N.

The selective photo-back reaction of M was also used in a time-resolved study at room temperature (56). The presence of M₁ and M₂ at early and late times was inferred from model calculations (30, 160) and from the different time constants obtained for the photo-back reaction of early and late M intermediates. The authors suggest a reaction sequence M → BR' → BR and that the measured difference spectra would represent M-BR'. Assuming that BR'₁ and BR'₂ are identical (a question not addressed by the authors), the fact that only minute differences were found in the M₁-BR'₁ and M₂-BR'₂ difference spectra would argue for only slight changes between M₁ and M₂. Consequently, the switch would involve only very small conformational changes. Both difference spectra resemble mostly M₁ or low-temperature (< 240° K) M of former work (110, 111, 119, 133, 164).

A comparative study (136) demonstrated that low temperature mimics the effect of low hydration, either in wt or the mutant D96N. The ratio of 1670 cm⁻¹/1660 cm⁻¹ absorption was found to be > 1 at high r.h./temperature but < 1 at low r.h./temperature. All spectra displayed an D85 band at 1761 cm⁻¹, although with a shoulder at lower wave numbers in case of D96N at r.h. > 75% and WT at 250° K. This band was completely shifted to 1755 cm⁻¹ in a sample of WT-BR incubated with guanidine hydrochloride at pH 9.6, and the negative band at 1670 cm⁻¹ was almost twice as large as in any other sample, and most specifically, a negative band at 1742 cm⁻¹ indicated a deprotonated D96. The proton must then be released toward the CP side of the membrane. It was argued that the ratio of 1670:1660 and the shape of the D85 band are

indicative for M_1 (ratio < 1 ; 1761 cm^{-1}) and M_2 (ratio > 1 ; 1761 with shoulder toward 1755) and the shift of the D85 band to 1755 cm^{-1} for the M_N state. Consequently, the M state of D96N at high pH was identified as M_2 with no significant contributions of M_N . Whereas the structural changes monitored by the ratio of $1670\text{ cm}^{-1}/1660\text{ cm}^{-1}$ continue beyond the M_2 state into M_N , those seen by X-ray diffraction are completed with the formation of M_2 (136; see below). In a study of the D38R mutant, the M state at pH 6.7 was found to be M_1 , whereas it was identified as M_2 at pH 9.6 with and without GuaHCl (135).

Taken together, the results from FTIR measurements have introduced a new intermediate M_N that suggests a reaction sequence of $L \rightarrow M_1 \rightarrow M_2 \rightarrow M_N \rightarrow N$. In M_N , the protein has adopted the conformation typical for the N intermediate, but the Schiff base is still deprotonated. It seems to be stabilized whenever there is no proton available to reprotonate the Schiff base, e.g. in the D96N mutant (133) or in the presence of GuaHCl or arginine (136), but does not accumulate in WT-BR. In summary, whether M_N as defined by FTIR experiments is a transient intermediate of the catalytic cycle of WT-BR or is specific to the conditions used to trap it is not known and needs further experimentation. The results of the FTIR studies are summarized in Table 2.

The crystalline nature of the PM allows the study of structural changes during the photocycle by diffraction methods, which provide the most direct evidence for global conformational changes. Namely, neutron (24, 50, 167) X-ray (72, 78, 106, 136) and electron diffraction (40, 148–150, 163) have been applied. Difference maps between illuminated and unilluminated samples allow the identification of projected areas with changed densities. It should be kept in mind, however, that most of the mutants introduce structural perturbations even in the dark state, which is evident from difference maps between unilluminated WT and mutant. The different mutants and experimental conditions used (summarized in Table 3) probably lead to the trapping of different photocycle intermediates or possibly even side products. In some cases, parallel FTIR difference spectra under similar conditions have been recorded that allow correlation with the M_1 , M_2 , and M_N intermediates defined by their specific difference bands. Otherwise, the trapped intermediate is inferred from other experiments (Table 3, last column).

Consistently, when the M_1 intermediate was trapped either by low temperature (40), low hydration (136, 167), or mutation D38R (136, 150), only very small changes were detected, hardly above the noise level. This was also true for the preceding L intermediate (55). Consequently, the catalytic cycle up to intermediate M_1 , in which the Schiff base proton is transferred to D85, is not associated with large conformational changes. In these cases, the ratio of the $1670/1660$ amide I bands is < 1 , as discussed above (compare; Table 2).

Table 2 Summary of spectral features used to characterize the different M species by Fourier transform infrared difference spectroscopy. +/- and the number of signs indicate the sign and (qualitatively) the amplitude of the respective band. *Sp*: species; *n*: narrow; *b*: broad; *s*: shoulder which indicates broadening toward 1755 cm⁻¹ in the case of D85H band, toward higher wave numbers in the case of the amide II band, and a shoulder to the 1670 cm⁻¹ band in the case of the 1660 cm⁻¹ amide I band; *calculated spectrum

Ref.	D85 [cm ⁻¹]	D96 [cm ⁻¹]	Amide I [cm ⁻¹]			Amide II [cm ⁻¹]	Sample	Sp.
			1670	1660	1650			
110	+1761	±0	---	----	-	+1564n	WT, 240° K	M ₁
	+1755	-1742	----	---	++	+1556b	WT, 260° K	M ₂
111	+1762	+1738	---	----	-	+1557b	WT, 220° K–270° K	M*
133	+1755	+1742	----	s.	++	+1557n	D96N, pH10	MN*
119	+1762	±0	---	----	-	+1560b	WT, 240° K, glucose, 81% r.h.	M ₁
	+1762	±0	----	---	++	+1560n	WT, 260° K, glucose, 81% r.h.	M ₂
164	+1761	±0	---	----	±0	+1566b	WT, 240° K, glucose, 81% r.h.	M
	+1761	±0	----	---	++	+1560n	WT, 260° K, glucose, 81% r.h.	M + M _N
56	+1761	+1738	---	----	-	+1554	WT, pH 7.5	M ₁
	+1761	+1738	---	----	-	+1554	WT, pH 7.5	M ₂
73	+1755	+1742	----	---	++	+1555n	D96N, pH 10, 100% r.h.	M _N
	+1762	+1742	---	----	±0	+1564b	D96N, pH 10, 75% r.h.	M ₂
136	+1761	+1742	---	----	-	+1569b	D96N, 38% r.h.	M ₁
							WT, 50% r.h.	M ₁
							WT, ≤240° K, 100% r.h.	M ₁
	+1761s	+1742	----	---	++	+1556n	D96N, ≥75% r.h.	M ₂
	+1755	-1742	----	s.	++	+1556n	WT, 250° K	M + N (M _G)
135	+1761	+1738	±0	-	±0	+1662b	D38R, pH 6.7	M ₁
	+1761s	-1742	----	s.	±0	+1556n	D38R, pH 9.6 ± GuaHCl	M ₂

Further development of M leads to changes in electron density mainly near helices B, G, and F (24, 45, 50, 55, 78, 106, 149), as found in studies using conditions that presumably trapped M_N (133). Using slightly tilted samples, these structural changes could be mostly confined to the cytoplasmic side of the membrane (149), which was confirmed for the N intermediate (163). In the case of D96G at high pH (148), it was suggested that ordering of the cytoplasmic part of helix G and an outward movement by 2 Å of helix F, possibly by pivoting

Table 3 Summary of structural changes observed with diffraction techniques. *Tech.*: applied technique; *e.d.*: electron diffraction; *n.d.*: neutron diffraction; *x.d.*: X-ray diffraction; *Sp.*: species; small/capital letters qualitatively indicate the extent of change found near the respective helices. Brackets indicate that the assignment of the intermediate is *not* based on accompanying FTIR measurements.

Ref.	Tech.	Sample	Light-induced changes near helices							Sp.
			A	B	C	D	E	F	G	
40	e.d.	WT, glucose embedded, dried					no change			[M ₁]
24	n.d.	WT., Gnd-HCl, high pH		b				F	G	[M _N]
106	x.d.	WT, arginine, high pH		B				f	G	[M _N]
78	x.d.	D96N, pH 9.6		b				F	G	[M ₂]
148	e.d.	D96G, pH 8.5			c	d	e	F	G	[M ₂]
		WT, 5°C	a	B					G	[M ₂]
50	n.d.	WT, Gnd-HCl, high pH						F	G	[M _N]
45	e.d.	WT, glucose embedded 240° K					E		G	M
		WT, glucose embedded 260° K		B				F	g	M + M _N
72	x.d.	F171C, 5°C						F	G	N
		D96N, pH11		B				F	G	[M _N]
163	e.d.	F219L		b				F	G	N
73	x.d.	D96N, pH 10, 76% r.h.		B				f	G	M ₂
		D96N, pH 10, 100% r.h.		b				F	G	M _N
136	x.d.	D96N, 15%–57% r.h.			c			g		M ₁
		D96N, 75%–100% r.h.		B				G	F	M ₂
149	e.d.	L93A, pH 5.2, 6°C		B	C	D		G	f	O _{cis}
166	n.d.	D96N, 57% r.h.					no change			[M ₁]
		D96N, 75% r.h.		B			e	F	G	[M ₂]
		D96N, 86% r.h.					e	F	G	[M ₂]
135	x.d.	D38R pH 6.7		b				f	g	M ₁
		D38R pH 9.6 ± GuaHCl						F	G	M ₂
150	e.d.	WT, pH 6.0, 5°C, 1 ms		B	c			f	G	[M]
		WT, pH 6.0, 5°C, 35 ms		B	c		e	f	G	[M, N]
		WT, pH 9.5, 5°C, 35 ms		B	c		e	f	G	[M, N]
		D96N, pH 6.0/9.5, 10 ms		B	c		e	F	G	[M _N]
		D96G, pH 6.0, 5°C, 150 ms		B	c			F	G	[M _N]
		F219L, 6 ms		b				f	G	[M]
		F219L, 35 ms		B	c		e	f	G	[N]
		D38R, 10 ms		b				f	g	[M ₁]
		T46V, pH 6.0, 5°C, 10 ms		B	c		e	f	G	[N]
		D96G, F171C, F219L					no change			[M, O]
55	e.d.	WT, glucose embedded, 170° K					no change			L
		WT, glucose embedded, 240° K		b		d	e	F	G	M + M _N

about Pro186, caused the density changes. The latter change was not found for WT-BR at 5°C, in which case M_2 might have been trapped.

Two studies determined conformational changes in the N intermediate that is selectively accumulated in mutants F219L (163) and F171C (72) as confirmed by FTIR difference and absorption spectroscopy, respectively. The difference density maps were found to be basically identical to those of the late M intermediate (24, 50, 106). Both find major changes in the vicinity of helices F and G and smaller ones near helix B. It is suggested that structural changes near helix B and G occur in the early M state (72). Assuming that the difference maps showing no significant changes (40, 136, 167) represent M_1 , it would follow that helix B and G change during the $M_1 \rightarrow M_2$ transition. Movement of helix F, on the other hand, replaces changes near helix B and is expected to occur with the $M_2 \rightarrow N$ and $M_2 \rightarrow M_N$ transition in wt and mutant D96N BR, respectively (72). This is confirmed in a study with D96N at different hydration levels (73). Changes at helices B, F, and G are found at hydration levels of both 100% r.h. and 75% r.h. However, changes near helix F were stronger compared to those near helix B in the case of a high level of hydration, while the opposite applied at a low hydration level. FTIR spectra under similar conditions showed the accumulation of M_2 and M_N at 75% and 100% r.h., respectively.

Changes in FTIR difference spectra were correlated with those seen in electron density difference maps (135, 136). The FTIR spectra have been discussed above (Table 2). For samples with a 1670/1660 ratio < 1 (D96N at $\leq 57\%$ r.h.; WT at 50% r.h.; WT at $\leq 240^\circ$ K), no changes were found, whereas in the case of 1670/1660 > 1 , changes near helices B, F, and G were detected. It was concluded that the large structural changes seen in the diffraction experiments occur in a single step from M_1 to M_2 (i.e. within the resolution of trapping experiments), whereas the FTIR bands in the amide I region develop more gradually from M_1 through M_2 to M_N . It is noted that infrared absorption coefficients may change considerably even upon small structural perturbations, leading to strong amplitudes of the difference bands, even though the global structural model doesn't change appreciably (e.g. in M_2 versus M_N).

In a comparative study using a special cryo trapping method, time-resolved structural changes of different mutants were compared to WT, both of the unilluminated state and of photo-intermediates (150). It is suggested that the same fundamental scheme of structural changes (e.g. near helices B, G, and F) is able to describe changes for WT and mutants. Differences detected between mutants and wt are interpreted as variations of that scheme rather than being specific for that particular mutant. Some mutants display structural perturbations even in the unilluminated state that mimic light-induced changes. Particularly interesting in this respect is the triple mutant D96G/F171C/F219L, the dark state of which shows almost the full extent of conformational changes normally

induced by light. No additional changes are found upon illumination, yet the mutant has a specific proton-transport activity similar to that of the WT (J Tittor & D Oesterhelt, unpublished). This proves that the switch resides not only in large protein conformational changes, as widely assumed, but at least partially in the retinal moiety. A different bending of the retinal polyene chain with protonated and unprotonated SB is suggested to be part of the switch (150).

A three-phase scenario is invoked to describe the components of the switch (73, 74). First, the connection of the SB to D85 is disrupted, followed by a reorientation toward the CP channel, and finally, an outward movement of helix F. The latter has been interpreted as a widening of the cytoplasmic channel, allowing water molecules to enter and interact with D96, thereby decreasing its pK and rendering it a proton donor (J Heberle, personal communication). The increased binding of water was also suggested by the specific deceleration of the $M_1 \rightarrow M_2$ step by osmotically active substances (19) and photothermal beam deflection measurements detecting a volume increase in M corresponding to 11 water molecules (139). The pressure dependence of rate constants suggested up to 20 bound water molecules in the later part of the photocycle (162), which is also compatible with expected volume changes from the increased lattice constant in M (24). However, a neutron diffraction study ruled out changes in the projected proton channel hydration exceeding 20% (167), which would account for less than 2 water molecules on the basis of the experimentally found 6–8 essential water molecules in the projection map (51).

Movement of helix F was also suggested by the effects of bulky groups coupled to engineered cysteines at the cytoplasmic ends of helices A to G (17). Only when helix F was labeled the reprotonation of the SB significantly was slowed down, while reprotonation of D96 was accelerated. Crosslinking of helix F with benzophenone, although unspecific, caused the opposite effects and seems to confirm the conclusion that movements of helix F strongly affect proton transfer rates. In a similar approach, WT and mutant D96N were treated with glutaraldehyde or LuCl_3 (123). The dependence of the azide-induced acceleration of the M-decay in D96N on azide concentration was shifted to higher azide concentrations. It was suggested that two M forms with different accessibilities of the SB for azide are in equilibrium and that the agents shift the equilibrium toward the less accessible M form.

Time-resolved electron spin resonance spectroscopy of BR labeled at the AB, CD, and EF loop detected a light-induced increase of the distance between the EF loop and either the AB or CD loop (147, 154). This increase is on the order of 5 Å and occurs with the decay of the M intermediate. This would be compatible with the structural studies, which found a large movement of helix F upon formation of M_N or N, respectively. The movements of loops,

on the other hand, do not necessarily reflect the conformational changes of helices.

Solid-state NMR (64) of isotopically labeled BR at low temperature demonstrated for the first time the actual interconversion of different M species, characterized by the distinct chemical shifts of their SB nitrogens, e.g. $M_o \rightarrow M_n + N \rightarrow BR$ (subscripts "o" and "n" stand for "old" and "new", not to be mistaken with intermediates O and N). M_o itself, however, was decomposed into two substates, M_{o1} and M_{o2} . On the basis of measurements of [$1-^{13}C$] Val-labeled BR, substantial structural changes were seen in the $M_o \rightarrow M_n$ transition that could be part of the reprotonation switch.

Photoelectric and absorbance measurements of the M back-reaction provided evidence for the existence of two M substates that gave rise to different kinetics of the response (25). The relative amplitude of the slower component increased with the delay of the second flash with respect to the first actinic flash, suggesting a linear reaction sequence of two M intermediates. Expression of BR in oocytes (104) and patch clamping the cell membrane allow the application of defined potentials across the membrane and recording of current-voltage curves. The current could be extrapolated to zero at a potential of -250 mV, which would represent the thermodynamic driving force of the proton pump, very close to the -280 mV found for the membrane potential of *H. salinarium* cells (97). It was found that the blue-light quenching effect strongly depends on the applied voltage. This was explained by an equilibrium between M_1 and M_2 , which is shifted toward M_1 upon application of a pump-inhibiting potential (103). Therefore, the switch $M_{cp} \rightarrow M_{ec}$ must be connected to a charge movement, although spectroscopic measurements have identified the $M \rightarrow BR$ as the major electrogenic step (28, 75). The large free energy decrease during the switch event of -250 mV is in accordance with an irreversible $M_1 \rightarrow M_2$ transition (158–160) but incompatible with a "flickering" between EC and CP accessibilities of the Schiff base, i.e. an equilibrium of M_1 and M_2 close to 1 (15, 86).

Completing the Cycle

The transition of the M to the N intermediate is chemically dominated by a proton transfer from D96 to the Schiff base; however, N must include two substates as reprotonation of D96 from CP occurs during its lifetime. The structural changes, as analyzed by X-rays or EM crystallography, during the $M_1 \rightarrow M_2$ transition persist in the N state, and additional secondary structural changes have been observed during M_2 -N transition as a changing ratio in the amide-I region (see above). The outward tilt of helix F in its cytoplasmic half was suggested to be caused by a hinge consisting of tyrosine 185 and proline 186 on the basis of site-specific labeling of tyrosine residues and the demonstration

that the carbonyl group of Y185 changes its position. The intermediate N was shown to be a 13-*cis* intermediate but must involve two substates because the reprotonation of D96 from the cytoplasmic surface occurs during its lifetime.

Electron crystallographic and X-ray diffraction experiments on the mutants F219L and F171C reveal the basic features of the cytoplasmic part of the helix F in the N intermediate (72, 163), as was seen before in D96G mutants. Although it might be that the early observed changes of helix G toward a more ordered structure occur before the tilt of helix F, all work on mutants is faced with the problem of possibly not reporting changes occurring in wild type. Thus, it has to be considered as an open question what the real structural changes are during the wild-type catalytic cycle. In any case, the N intermediate exhibits all features of a large structural change reported for late M intermediates. Chemically, the N intermediate is characterized by the 13-*cis* configuration of the chromophore and its capacity to photochemically revert to BR as do the intermediates K, L, and M (91).

The N \rightarrow O transition, after reprotonation of D96, is considered as the 13-*cis* to all-*trans* isomerization of retinal in the environment of a protonated D85 (144). The attempt to prolong the lifetime of the O intermediate for structural studies leads to intensive investigation of the L93A mutant of BR, which produces a red-shifted long-living intermediate in the photocycle and which, however, was shown to contain a 13-*cis* intermediate (23) and to conserve the structural changes occurring in the M-state. This leaves the question of the exact time point of isomerization of retinal in wild type as an unsolved problem. The O intermediate itself in wild type is characterized by its preferential occurrence at high temperatures due to the activation energy barriers of conversion to BR initial state. It exhibits an unusual photochemical reaction of low quantum yield, e.g. a conversion to 9-*cis* retinal. This isomer is formed at the expense of all *trans* retinal, not 13-*cis* retinal as shown by extraction analysis (122a). This might be used as an additional argument for O in wild type as being *trans*, because mutants in the D85 position showing the same absorption maximum as the O intermediate are also converted in a photochemical reaction to the persisting photoproduct 9-*cis*. This becomes interesting for possible technical application as a thermally stable state.

After *cis-trans* isomerization, the BR molecule deprotonates D85H, restoring the protonation state of the EC H-bonded network, and the protein conformation returns in its initial state. It is unclear whether release of a proton from D85 or the conformational rechange to the initial state is the immediate consequence of the thermal isomerization step.

Much information has been compiled over the past 28 years; no doubt this molecule is now the best characterized active ion translocator. However, its structure is not solved to atomic resolution, and the structural changes

responsible for the accessibility change of the active center for protons are not known. Further, the time-resolved migration of protons along the conduction pathways in the structure has eluded a complete description so far. For this, knowledge of the complete structural dynamics of the molecule is required.

Visit the *Annual Reviews* home page at
<http://www.AnnualReviews.org>

Literature Cited

1. Akiyama R, Yoshimori A, Kakitani T, Imamoto Y, Shichida Y, Hatano Y. 1997. Analysis of the excited state dynamics of 13-trans locked bacteriorhodopsin. *J. Phys. Chem.* 101:412–17
2. Alexiev U, Mollaahabada R, Scherrer P, Khorana HG, Heyn MP. 1995. Rapid long-range proton diffusion along the surface of the purple membrane and delayed proton transfer into the bulk. *Proc. Natl. Acad. Sci. USA* 92:372–76
3. Ames JB, Mathies RA. 1990. The role of back-reactions and proton uptake during the N → O transition in bacteriorhodopsin's photocycle: a kinetic resonance Raman study. *Biochemistry* 29:7181–90
4. Aton B, Doukas AG, Callender RH, Becher B, Ebrey TG. 1977. Resonance Raman studies of purple membrane. *Biochemistry* 16:2995–99
5. Bamberg E, Tittor J, Oesterhelt D. 1993. Light-driven proton or chloride pumping by halorhodopsin. *Proc. Natl. Acad. Sci. USA* 90:639–43
6. Bashford D, Gerwert K. 1992. Electrostatic calculations of the pKa values of ionizable groups in bacteriorhodopsin. *J. Mol. Biol.* 224:473–86
7. Bogomolni R, Stoeckenius W, Szundi I, Perozo E, Olson KD, Spudich JL. 1994. Removal of transducer HtrI allows electrogenic proton translocation by sensory rhodopsin I. *Proc. Natl. Acad. Sci. USA* 91:10188–92
8. Booth PJ, Farooq A. 1997. Intermediates in the assembly of bacteriorhodopsin investigated by time-resolved absorption spectroscopy. *Eur. J. Biochem.* 246:674–80
9. Booth PJ, Farooq A, Flitsch SL. 1996. Retinal binding during folding and assembly of the membrane protein bacteriorhodopsin. *Biochemistry* 35:5902–9
10. Booth PJ, Flitsch SL, Stern LJ, Greenhalgh DA, Kim PS, Khorana HG. 1995. Intermediates in the folding of the membrane protein bacteriorhodopsin. *Struct. Biol.* 2:139–43
11. Booth PJ, Paulsen H. 1996. Assembly of the light harvesting chlorophyll a/b complex in vitro—Time resolved fluorescence measurements. *Biochemistry* 35:5103–8
12. Booth PJ, Riley ML, Flitsch SL, Temple RH, Farooq A, et al. 1997. Evidence that bilayer formation bending rigidity affects membrane protein folding. *Biochemistry* 36:197–203
13. Brack TL, Atkinson GH. 1991. Vibrationally excited retinal in the bacteriorhodopsin photocycle: picosecond time-resolved anti-Stokes Resonance Raman scattering. *J. Phys. Chem.* 95:2351–56
14. Braiman MS, Dioumaev AK, Lewis JR. 1996. A large photolysis-induced pKa increase of the chromophore counterion in bacteriorhodopsin: implications for ion transport mechanisms of retinal proteins. *Biophys. J.* 70:939–47
15. Brown LS, Dioumaev AK, Needleman R, Lanyi JK. 1998. Local-access model for proton transfer in bacteriorhodopsin. *Biochemistry* 37:3982–93
16. Brown LS, Lanyi JK. 1996. Determination of the transiently lowered pKa of the retinal Schiff base during the photocycle of bacteriorhodopsin. *Proc. Natl. Acad. Sci. USA* 93:1731–34
17. Brown LS, Varo G, Needleman R, Lanyi JK. 1995. Functional significance of a protein conformation change at the cytoplasmic end of helix F during the bacteriorhodopsin photocycle. *Biophys. J.* 69:2103–11
18. Butt HJ, Fendler K, Bamberg E, Tittor J, Oesterhelt D. 1989. Aspartic acids 96 and 85 play a central role in the function of bacteriorhodopsin as a proton pump. *EMBO J.* 8:1657–63
19. Cao Y, Varo G, Chang B, Ni B, Needleman R, Lanyi JK. 1991. Water is required for proton transfer from aspartate

- 96 to the bacteriorhodopsin Schiff base. *Biochemistry* 30:10972–79
20. Chekover S, Nachliel E, Dencher NA, Gutman M. 1997. Mechanism of proton entry into the cytoplasmic section of the proton conducting channel of bacteriorhodopsin. *Biochemistry* 36:13919–28
 21. Cordfunke R, Kort R, Pierik A, Gobets B, Koomen GJ, et al. 1998. Trans/cis (Z/E) photoisomerization of the chromophore of photoactive yellow protein is not a prerequisite for the initiation of the photocycle of this protein. *Proc. Natl. Acad. Sci. USA* 95:7396–401
 22. Delaney JK, Brack TL, Atkinson GH, Ottolenghi M, Steinberg G, Sheves M. 1995. Primary picosecond molecular events in the photoreaction of the BR5.12 artificial bacteriorhodopsin pigment. *Proc. Natl. Acad. Sci. USA* 92:2101–5
 23. Delaney JK, Schweiger U, Subramaniam S. 1995. Molecular mechanism of protein-retinal coupling in bacteriorhodopsin. *Proc. Natl. Acad. Sci. USA* 92:11120–24
 24. Dencher NA, Dresselhaus D, Zaccai G, Büldt G. 1989. Structural changes in bacteriorhodopsin during proton translocation revealed by neutron diffraction. *Proc. Natl. Acad. Sci. USA* 86:7876–79
 25. Dickopf S, Heyn MP. 1997. Evidence for the first phase of the reprotonation switch of bacteriorhodopsin from time-resolved photovoltage and flash photolysis experiments on the photoreversal of the M-intermediate. *Biophys. J.* 73:3171–81
 26. Döbler J, Zinth W, Kaiser W, Oesterheld D. 1988. Excited-state reaction dynamics of bacteriorhodopsin studied by femtosecond spectroscopy. *Chem. Phys. Lett.* 144:215–20
 27. Doig SJ, Reid PJ, Mathies RA. 1991. Picosecond time-resolved resonance Raman spectroscopy of Bacteriorhodopsin's J, K, and KL intermediates. *J. Phys. Chem.* 95:6372–79
 28. Drachev LA, Kaulen AD, Khitrina LV, Skulachev VP. 1981. Fast stages of photoelectric processes in biological membranes. *Eur. J. Biochem.* 117:461–70
 29. Dracheva S, Bose S, Hendler RW. 1996. Chemical and functional studies on the importance of purple membrane lipids in bacteriorhodopsin photocycle behavior. *FEBS Lett.* 382:209–12
 30. Druckmann S, Friedman N, Lanyi JK, Needleman R, Ottolenghi M, Sheves M. 1992. The back reaction of the M intermediate in the photocycle of bacteriorhodopsin: mechanism and evidence for two M species. *Photochem. Photobiol.* 56:1041–47
 31. Du M, Fleming GR. 1993. Femtosecond time-resolved fluorescence spectroscopy of bacteriorhodopsin: direct observation of excited state dynamics in the primary step of the proton pump cycle. *Biophys. Chem.* 48:101–11
 32. Essen LO, Siebert R, Lehmann WD, Oesterheld D. 1998. Lipid patches in membrane protein oligomers: crystal structure of the bacteriorhodopsin-lipid complex. *Proc. Natl. Acad. Sci. USA* 95:11673–78
 33. Fischer U, Oesterheld D. 1980. Changes in the protonation state of bacteriorhodopsin during reconstitution of bacteriorhodopsin. *Biophys. J.* 31:139–46
 34. Fischer U, Towner P, Oesterheld D. 1981. Light induced isomerization at acidic pH initiates hydrolysis of bacteriorhodopsin to bacterio-opsin and 9-cis retinal. *Photochem. Photobiol.* 33:529–37
 35. Fitter J, Verclas SAW, Lechner RE, Seelert H, Dencher NA. 1998. Function and picosecond dynamics of bacteriorhodopsin in purple membrane at different lipidation and hydration. *FEBS Lett.* 433:321–25
 36. Fodor SPA, Ames JB, Gebhard R, vanden Berg EMM, Stoeckenius W, et al. 1988. Chromophore structure in bacteriorhodopsin's N intermediate: implications for the proton-pumping mechanism. *Biochemistry* 27:7097–100
 37. Fu X, Bressler S, Ottolenghi M, Eliash T, Friedman N, Sheves M. 1997. Titration kinetics of asp-85 in bacteriorhodopsin: exclusion of the retinal pocket as the color-controlling cation binding site. *FEBS Lett.* 416:167–70
 38. Gai F, Hasson KC, McDonald JC, Anfinrud PA. 1998. Chemical dynamics in proteins: the photoisomerization of retinal in bacteriorhodopsin. *Science* 279:1886–91
 39. Gerwert K, Siebert F. 1986. Evidence for light-induced 13-cis 14-s-cis isomerization in bacteriorhodopsin obtained by FTIR difference spectroscopy using isotopically labelled retinals. *EMBO J.* 5:805–11
 40. Glaeser RM, Baldwin J, Ceska TA, Henderson R. 1986. Electron diffraction analysis of the M412 intermediate of bacteriorhodopsin. *Biophys. J.* 50:913–20
 41. Govindjee R, Balashov S, Ebrey T, Oesterheld D, Steinberg G, Sheves M. 1994. Lowering the intrinsic pKa of the chromophore

- mophore's Schiff base can restore its light-induced deprotonation in the inactive Tyr57 → asn mutant of bacteriorhodopsin. *J. Biol. Chem.* 269:14353–54
42. Grigorieff N, Beckmann E, Zemlin F. 1995. Lipid location in deoxycholate-treated purple membrane at 2.6 Å. *J. Mol. Biol.* 254:404–15
 43. Grigorieff N, Ceska TA, Downing KH, Baldwin JM, Henderson R. 1996. Electron-crystallographic refinement of the structure of bacteriorhodopsin. *J. Mol. Biol.* 259:393–21
 44. Hage W, Kim M, Frei H, Mathies RA. 1996. Protein dynamics in the bacteriorhodopsin photocycle: a nanosecond step-scan FTIR investigation of the KL to L transition. *J. Phys. Chem.* 100:16026–33
 45. Han BG, Vonck J, Glaeser RM. 1994. The bacteriorhodopsin photocycle: direct structural study of two substates of the M-intermediate. *Biophys. J.* 67:1179–86
 46. Haran G, Wynne K, Xie A, He Q, Chance M, Hochstrasser RM. 1996. Excited state dynamics of bacteriorhodopsin revealed by transient stimulated emission spectra. *Chem. Phys. Lett.* 261:389–95
 47. Hasson KC, Gai F, Anfinrud PA. 1996. The photoisomerization of retinal in bacteriorhodopsin: experimental evidence for a three-state model. *Proc. Natl. Acad. Sci. USA* 93:15124–29
 48. Haupts U, Bamberg E, Oesterheld D. 1996. Different modes of proton translocation by sensory rhodopsin I. *EMBO J.* 15:1834–41
 49. Haupts U, Haupts C, Oesterheld D. 1995. The photosensory rhodopsin I as a two-photon-driven proton pump. *Proc. Natl. Acad. Sci. USA* 92:3834–38
 50. Hauss T, Büldt G, Heyn MP, Dencher NA. 1994. Light-induced isomerization causes an increase in the chromophore tilt in the M intermediate of bacteriorhodopsin: a neutron diffraction study. *Proc. Natl. Acad. Sci. USA* 91:11854–58
 51. Hauss T, Papadopoulos G, Verclas SAW, Büldt G, Dencher NA. 1997. Neutron diffraction on purple membranes: essential water molecules in the light-driven proton pump bacteriorhodopsin. *Physica B* 234:217–19
 52. Heberle J, Dencher NA. 1992. Surface-bound optical probes monitor proton translocation and surface potential changes during the bacteriorhodopsin photocycle. *Proc. Natl. Acad. Sci. USA* 89:5996–6000
 53. Heberle J, Riesle J, Thiedemann G, Oesterheld D, Dencher NA. 1994. Proton migration along the membrane surface and retarded surface to bulk transfer. *Nature* 370:379–82
 54. Henderson R, Baldwin JM, Ceska TA, Zemlin F, Beckmann E, Downing KH. 1990. Model for the structure of bacteriorhodopsin based on high-resolution electron cryo-microscopy. *J. Mol. Biol.* 213:899–929
 55. Hendrickson FM, Burkard F, Glaeser RM. 1998. Structural characterization of the L-to-M transition of the bacteriorhodopsin photocycle. *Biophys. J.* 75:1446–54
 56. Hessling B, Herbst J, Rammelsberg R, Gerwert K. 1997. Fourier transform infrared double-flash experiments resolve bacteriorhodopsin's M1 to M2 transition. *Biophys. J.* 73:2071–80
 57. Hessling B, Souvignier G, Gerwert K. 1993. A model independent approach to assigning bacteriorhodopsin's intramolecular reactions to photocycle intermediates. *Biophys. J.* 65:1929–41
 58. Heyman J, Jager R, Subramaniam S. 1997. Expression of bacteriorhodopsin in Sf9 and COS-1 cells. *J. Bioenerg. Biomembr.* 29:55–59
 59. Hildebrandt P, Stockburger M. 1984. Role of water in the bacteriorhodopsin chromophore: a resonance Raman study. *Biochemistry* 23:5539–48
 60. Hildebrandt V, Ramezani-Rad M, Swida U, Wrede P, Grzesiek S, et al. 1989. Genetic transfer of the pigment bacteriorhodopsin into the eukaryote *Schizosaccharomyces pombe*. *FEBS Lett.* 243:137–40
 61. Hoff WD, Jung KH, Spudis JL. 1997. Molecular mechanism of photosignaling by archaeal sensory rhodopsins. *Annu. Rev. Biophys. Biomol. Struct.* 26:223–58
 62. Holz M, Drachev LA, Mogi T, Otto H, Kaulen AD, et al. 1989. Replacement of aspartic acid-96 by asparagine in bacteriorhodopsin slows both the decay of the M-intermediate and the associated proton movement. *Proc. Natl. Acad. Sci. USA* 86:2167–71
 63. Hu JG, Griffin RG, Herzfeld J. 1997. Interactions between the protonated Schiff base and its counterion in the photointermediates of bacteriorhodopsin. *J. Am. Chem. Soc.* 119:9495–98
 64. Hu JG, Sun BQ, Bizounok M, Hatcher ME, Lansing JC, et al. 1998. Early and late intermediates in the bacteriorhodopsin photocycle: a solid-state NMR study. *Biochemistry* 37:8088–96

65. Hu JGG, Sun BQQ, Petkova AT, Griffin RG, Herzfeld J. 1997. The predischARGE chromophore in bacteriorhodopsin: a ¹⁵N solid state NMR study of the L photointermediate. *Biochemistry* 36:9316–22
66. Huang KS, Bayley H, Liao MJ, London E, Khorana HG. 1981. Refolding of an integral membrane protein. *J. Biol. Chem.* 256:3802–9
67. Hunt JF, Earnest TN, Bousche O, Kalgatgi K, Reilly K, et al. 1997. A biophysical study of integral membrane protein folding. *Biochemistry* 36:15156–76
68. Hunt JF, Rath P, Rotschild KJ, Engelman DM. 1997. Spontaneous pH-dependent membrane insertion of a transbilayer α -helix. *Biochemistry* 36:15177–92
69. Jonas R, Ebrey TG. 1991. Binding of a single divalent cation directly correlates with the blue-to-purple transition in bacteriorhodopsin. *Proc. Natl. Acad. Sci. USA* 88:149–53
70. Kahn TW, Engelman DM. 1992. Bacteriorhodopsin can be refolded from two independent stable transmembrane helices and the complementary five-helix segment. *Biochemistry* 31:6144–51
71. Kahn TW, Sturtevant JM, Engelman DM. 1992. Thermodynamic measurements of the contributions of helix-connecting loops and of retinal to the stability of bacteriorhodopsin. *Biochemistry* 31:8829–39
72. Kamikubo H, Kataoka M, Varo G, Oka T, Tokunaga F, et al. 1996. Structure of the N intermediate of bacteriorhodopsin revealed by X-ray diffraction. *Proc. Natl. Acad. Sci. USA* 93:1386–90
73. Kamikubo H, Oka T, Imamoto Y, Tokunaga F, Lanyi JK, Kataoka M. 1997. The last phase of the reprotonation switch in bacteriorhodopsin: the transition between the M-type and the N-type protein conformation depends on hydration. *Biochemistry* 36:12282–87
74. Kandori H, Yamazaki Y, Sasaki J, Needleman R, Lanyi JK, Maeda A. 1995. Water-mediated proton transfer in proteins: an FTIR study of bacteriorhodopsin. *J. Am. Chem. Soc.* 117:2118–19
75. Keszthelyi L, Ormos P. 1980. Electric signals associated with the photocycle of bacteriorhodopsin. *FEBS Lett.* 109:189–93
76. Kimura Y, Ikegami A, Stoerkenius W. 1984. Salt and pH-dependent changes of the purple membrane absorption spectrum. *Photochem. Photobiol.* 40:641–46
77. Kimura Y, Vassilyev DG, Miyazawa A, Kidera A, Matsushima M, et al. 1997. Surface of bacteriorhodopsin by high-resolution electron crystallography. *Nature* 389:206–10
78. Koch MHJ, Dencher NA, Oesterhelt D, Plöhn HJ, Rapp G, Büldt G. 1991. Time-resolved X-ray diffraction study of structural changes associated with the photocycle of bacteriorhodopsin. *EMBO J.* 10:521–26
79. Kollbach G, Steinmüller S, Berndsen T, Buss V, Gärtner W. 1998. The chromophore induces a correct folding of the polypeptide chain of bacteriorhodopsin. *Biochemistry* 37:8227–32
80. Korenstein R, Hess B. 1977. Hydration effects on the photocycle of bacteriorhodopsin in thin layers of purple membrane. *Nature* 270:184–86
81. Krebs MP, Khorana HG. 1993. Mechanism of light-dependent proton translocation by bacteriorhodopsin. *J. Bacteriol.* 175:1555–60
82. Krebs MP, Li W, Halambeck TP. 1998. Intramembrane substitutions in Helix D of bacteriorhodopsin disrupt the purple membrane. *J. Mol. Biol.* 267:172–83
83. Lanyi JK. 1994. Proton translocation mechanism and energetics in the light-driven pump bacteriorhodopsin. *Biochim. Biophys. Acta* 1183:241–61
84. Lanyi JK. 1995. Bacteriorhodopsin as a model for proton pumps. *Nature* 375:461–63
85. Lanyi JK. 1997. Mechanism of ion transport across membranes. *J. Biol. Chem.* 272:31209–12
86. Lanyi JK. 1998. The local-access mechanism of proton transport by bacteriorhodopsin. *Biochim. Biophys. Acta* 1365:17–22
87. Lanyi JK, Varo G. 1995. The photocycles of bacteriorhodopsin. *Isr. J. Chem.* 35:365–85
88. LeCoutre J, Tittor J, Oesterhelt D, Gerwert K. 1995. Experimental evidence for hydrogen-bonded network proton transfer in bacteriorhodopsin shown by Fourier-transform infrared spectroscopy using azide as catalyst. *Proc. Natl. Acad. Sci. USA* 92:4962–66
89. Logunov SL, Masciangioli TM, Kamalov VF, El-Sayed MA. 1998. Low-temperature retinal photoisomerization dynamics in bacteriorhodopsin. *J. Phys. Chem.* 102:2303–6
90. London E, Khorana HG. 1982. Denaturation and renaturation of bacteriorhodopsin in detergents and lipid-detergent mixtures. *J. Biol. Chem.* 257:7003–11

91. Ludlam CFC, Sonar S, Lee CP, Coleman M, Herzfeld J, et al. 1995. Site-directed isotope labeling and ATR-FTIR difference spectroscopy of bacteriorhodopsin: the peptide carbonyl group of tyr-185 is structurally active during the BR → N transition. *Biochemistry* 34:2–6
92. Luecke H, Richter HT, Lanyi JK. 1998. Proton transfer pathways in bacteriorhodopsin at 2.3 Ångstrom resolution. *Science* 280:1934–37
93. Maeda A, Iwasa T, Yoshizawa T. 1980. Formation of 9-*cis* and 11-*cis*-retinal pigments from bacteriorhodopsin by irradiating purple membrane in acid. *Biochemistry* 19:3825–31
94. Maeda A, Kandori H, Yamazaki Y, Nishimura S, Hatanaka M, et al. 1997. Intramembrane signaling mediated by hydrogen-bonding of water and carboxyl groups in bacteriorhodopsin and rhodopsin. *J. Biochem.* 121:399–406
95. Marti T. 1997. Refolding of bacteriorhodopsin from expressed polypeptide fragments. *J. Biol. Chem.* 273:9312–22
96. Mathies RA, Brito Cruz CH, Pollard WT, Shank CV. 1988. Direct observation of the femtosecond excited-state *cis-trans* isomerisation in bacteriorhodopsin. *Science* 279:277–79
97. Michel H, Oesterhelt D. 1976. Light-induced changes of the pH gradient and the membrane potential in *Halobacterium halobium*. *FEBS Lett.* 65:175–78
98. Milder SJ, Kligler DS. 1988. A time-resolved spectral study of the K and KL intermediates of bacteriorhodopsin. *Biophys. J.* 53:465–68
99. Miller A, Oesterhelt D. 1990. Kinetic optimization of bacteriorhodopsin by aspartic acid 96 as an internal proton donor. *Biochim. Biophys. Acta* 1020:57–64
100. Mukhopadhyay AK, Dracheva S, Bose S, Hendler RW. 1996. Control of the integral membrane proton pump bacteriorhodopsin by purple membrane lipids of *Halobacterium halobium*. *Biochemistry* 35:9245–52
101. Mukohata Y. 1994. Comparative studies on ion pumps of the bacterial rhodopsin family. *Biophys. Chem.* 50:191–201
102. Nachliel E, Yaniv-Checover S, Gutman M. 1997. The role of the surface group in funneling of protons towards the protonic channel of bacteriorhodopsin. *Solid State Ionics* 97:75–82
103. Nagel G, Kelety B, Möckel B, Büldt G, Bamberg E. 1998. Voltage dependence of proton pumping by bacteriorhodopsin is regulated by the voltage sensitive ratio of M1 to M2. *Biophys. J.* 68:403–12
104. Nagel G, Möckel B, Büldt G, Bamberg E. 1995. Functional expression of bacteriorhodopsin in oocytes allows direct measurement of voltage dependence of light induced H⁺ pumping. *FEBS Lett.* 377:263–66
105. Nagle JF. 1991. Photocycle kinetics: analysis of Raman data from bacteriorhodopsin. *Photochem. Photobiol.* 54:897–903
106. Nakasako M, Kataoka M, Amemiya Y, Tokunaga F. 1991. Crystallographic characterization by X-ray diffraction of the M-intermediate from the photo-cycle of bacteriorhodopsin at room temperature. *FEBS Lett.* 292:73–75
107. Nonella M, Windemuth A, Schulten K. 1991. Structure of bacteriorhodopsin and in situ isomerization of retinal: a molecular dynamics study. *Photochem. Photobiol.* 54:937–48
108. Oesterhelt D. 1995. Structure and function of halorhodopsin. *Isr. J. Chem.* 35:475–94
109. Oesterhelt D. 1998. The structure and mechanism of the family of retinal proteins from halophilic archaea. *Curr. Opin. Struct. Biol.* 8:489–500
110. Ormos P. 1991. Infrared spectroscopic demonstration of a conformational change in bacteriorhodopsin involved in proton pumping. *Proc. Natl. Acad. Sci. USA* 88:473–77
111. Ormos P, Chu K, Mourant J. 1992. Infrared study of the L, M, and N intermediates of bacteriorhodopsin using the photoreaction of M. *Biochemistry* 31:6933–37
112. Ottolenghi M, Sheves M. 1995. Photo-physics and photochemistry of retinal proteins. *Isr. J. Chem.* 35(3–4):U3
113. Ozawa S, Hayashi R, Masuda A, Iio T, Takahashi S. 1997. Reconstitution of bacteriorhodopsin from a mixture of a proteinase V8 fragment and two synthetic peptides. *Biochim. Biophys. Acta* 1323:145–53
114. Papadopoulos G, Dencher NA, Zaccai G, Büldt G. 1990. Water molecules and exchangeable hydrogen ions at the active center of bacteriorhodopsin localized by neutron diffraction. *J. Mol. Biol.* 214:15–19
115. Pardo L, Sepulcre F, Cladera J, Dunach M, Labarta A, et al. 1998. Experimental and theoretical characterization of the high-affinity cation-binding site of the purple membrane. *Biophys. J.* 75:777–84

116. Patzelt H, Ulrich AS, Egbrinchoff H, Düx P, Ashurst J, et al. 1997. Towards structural investigations on isotope labelled native bacteriorhodopsin in detergent micelles by solution-state NMR spectroscopy. *J. Biomol. NMR* 10:95–106
117. Pebay-Peyroula E, Rummel G, Rosenbusch JP, Landau EM. 1997. X-ray structure of bacteriorhodopsin at 2.5 Ångstroms from microcrystals grown in lipidic cubic phases. *Science* 277:1676–81
118. Perkins GA, Burkard F, Liu E, Glaeser RM. 1993. Glucose alone does not completely hydrate bacteriorhodopsin in glucose-embedded purple membrane. *J. Microsc.* 169:61–65
119. Perkins GA, Liu E, Burkard F, Berry EA, Glaeser RM. 1992. Characterization of the conformational change in the M1 and M2 substates of bacteriorhodopsin by the combined use of visible and infrared spectroscopy. *J. Struct. Biol.* 109:142–51
120. Polland HJ, Franz MA, Zinth W, Kaiser W, Kölling E, Oesterheld D. 1986. Early picosecond events in the photocycle of bacteriorhodopsin. *Biophys. J.* 49:651–62
121. Pomerleau V, Harvey-Girard E, Boucher F. 1995. Lipid-protein interactions in the purple membrane: structural specificity within the hydrophobic domain. *Biochim. Biophys. Acta* 1234:221–24
122. Popot JL, Engelman DM. 1990. Membrane protein folding and oligomerisation: the two-stage model. *Biochemistry* 29:4031–37
- 122a. Popp A, Wolperdinger M, Hampp N, Bräuchle C, Oesterheld D. 1993. Photochemical conversion of the O-intermediate to 9-cis retinal containing products in bacteriorhodopsin films. *Biophys. J.* 65:1449–59
123. Radionov AN, Kaulen AD. 1996. Two bacteriorhodopsin M intermediates differing in accessibility of the Schiff base for azide. *FEBS Lett.* 387:122–26
124. Rammelsberg R, Huhn G, Lübben M, Gerwert K. 1998. Bacteriorhodopsin's intramolecular proton-release pathway consists of a hydrogen-bonded network. *Biochemistry* 37:5001–9
125. Reat V, Patzelt H, Ferrand M, Pfister C, Oesterheld D, Zaccai G. 1998. Dynamics of different functional parts of bacteriorhodopsin: H-2H labeling and neutron scattering. *Proc. Natl. Acad. Sci. USA* 95:4970–75
126. Riley ML, Wallace BA, Flitsch SL, Booth PJ. 1997. Slow alpha-helix formation during folding of a membrane protein. *Biochemistry* 36:192–96
127. Rouso I, Brodsky I, Lewis A, Sheves M. 1995. The role of water in retinal complexation to bacterio-opsin. *J. Biol. Chem.* 270:13860–68
128. Rouso I, Friedman N, Lewis A, Sheves M. 1997. Evidence for a controlling role of water in producing the native bacteriorhodopsin structure. *Biophys. J.* 73:2081–89
129. Rouso I, Gat Y, Lewis A, Sheves M, Ottolenghi M. 1998. Effective light-induced hydroxylamine reactions occur with C13=C14 nonisomerizable bacteriorhodopsin pigments. *Biophys. J.* 75:413–17
130. Rouso I, Khachatryan E, Gat Y, Brodsky I, Ottolenghi M, et al. 1997. Microsecond atomic force sensing of protein conformational dynamics: implications for the primary light-induced events in bacteriorhodopsin. *Proc. Natl. Acad. Sci. USA* 94:7937–41
131. Rüdiger M, Tittor J, Gerwert K, Oesterheld D. 1997. Reconstitution of bacteriorhodopsin from the apoprotein and retinal studied by Fourier-transform infrared spectroscopy. *Biochemistry* 36:4867–74
132. Sampogna RV, Honig B. 1996. Electrostatic coupling between retinal isomerization and the ionization state of glu204: a general mechanism for proton release in bacteriorhodopsin. *Biophys. J.* 71:1165–71
- 132a. Sasaki J, Brown LS, Chon YS, Kandori H, Maeda A, Needleman R, Lanyi JK. 1995. Conversion of bacteriorhodopsin into a chloride pump. *Science* 269:73–75
133. Sasaki J, Shichida Y, Lanyi JK, Maeda A. 1992. Protein changes associated with reprotonation of the Schiff base in the photocycle of Asp96Asn bacteriorhodopsin. *J. Biol. Chem.* 267:20782–88
134. Sasaki J, Yuzawa T, Kandori H, Maeda A, Hamaguchi H. 1995. Nanosecond time-resolved infrared spectroscopy distinguishes two K species in the bacteriorhodopsin photocycle. *Biophys. J.* 68:2073–80
135. Sass HJ, Gessenich R, Koch MHJ, Oesterheld D, Dencher NA, et al. 1998. Evidence for charge-controlled conformation changes in the photocycle of bacteriorhodopsin. *Biophys. J.* 75:399–405
136. Sass HJ, Schachowa IW, Rapp G, Koch MHJ, Oesterheld D, et al. 1997. The

- tertiary structural changes in bacteriorhodopsin occur between M states. X-ray diffraction and Fourier transform infrared spectroscopy. *EMBO J.* 16:1484–91
137. Schreckenbach T, Walckhoff B, Oesterheld D. 1977. Studies on the retinal-protein interaction in bacteriorhodopsin. *Eur. J. Biochem.* 76:499–511
138. Schreckenbach T, Walckhoff B, Oesterheld D. 1978. Properties of the retinal binding site in bacteriorhodopsin: use of retinol and retinyl moieties as fluorescent probes. *Photochem. Photobiol.* 28:205–11
139. Schulenberg PJ, Rohr M, Gärtner W, Braslavsky SE. 1994. Photoinduced volume changes associated with the early transformations of bacteriorhodopsin: a laser induced optoacoustic spectroscopy study. *Biophys. J.* 66:838–43
140. Schulten K, Tavan P. 1978. A mechanism for the light-driven proton pump of *Halobacterium halobium*. *Nature* 272:85–86
141. Schweiger U, Tittor J, Oesterheld D. 1994. Bacteriorhodopsin can function without a covalent linkage between retinal and protein. *Biochemistry* 33:535–41
142. Shichida Y, Matuoka S, Hidica Y, Yoshizawa T. 1983. Absorption spectra of intermediates of bacteriorhodopsin measured at room temperature. *Biochim. Biophys. Acta* 723:240–46
143. Sing AK, Majumdar N. 1997. Role of metal cations in color transition and hydrolysis of the chromophores of retinal-binding photoreceptor proteins. *J. Photochem. Photobiol. B* 39:140–45
144. Smith SO, Pardo JA, Mulder PPJ, Curry B, Lugtenburg J, Mathies RA. 1983. Chromophore structure in bacteriorhodopsin's O640 intermediate. *Biochemistry* 22:6141–48
145. Sonar S, Marti T, Rath P, Fischer W, Coleman M, et al. 1994. A redirected proton pathway in the bacteriorhodopsin mutant Tyr57 → Asp. *J. Biol. Chem.* 269:28851–58
146. Spudich JL. 1998. Variations on a molecular switch: transport and sensory signalling by achaeal rhodopsins. *Mol. Microbiol.* 28:1051–58
147. Steinhoff HJ, Mollaaghababa R, Altenbach C, Hideg K, Krebs M, et al. 1994. Time-resolved detection of structural changes during the photocycle of spin-labeled bacteriorhodopsin. *Science* 266:105–7
148. Subramaniam S, Faruqi AR, Oesterheld D, Henderson R. 1997. Electron diffraction changes in the Leu93Ala bacteriorhodopsin mutant. *Proc. Natl. Acad. Sci. USA* 94:1767–72
149. Subramaniam S, Gerstein M, Oesterheld D, Henderson R. 1993. Electron diffraction analysis of structural changes in the photocycle of bacteriorhodopsin. *EMBO J.* 12:1–8
150. Subramaniam S, Lindahl M, Bullogh P, Faruqi W, Tittor J, et al. 1998. Protein conformational changes in the bacteriorhodopsin photocycle. *J. Mol. Biol.* In press
151. Surrey T, Jähnig F. 1995. Kinetics of folding and membrane insertion of a B-barrel membrane protein. *J. Biol. Chem.* 270:28199–203
152. Szundi I, Stoeckenius W. 1989. Surface pH controls purple-to-blue transition of bacteriorhodopsin. A theoretical model of purple membrane surface. *Biophys. J.* 56:369–83
153. Tan EHL, Govender DSK, Birge RR. 1996. Large organic cations can replace Mg²⁺ and Ca²⁺ ions in bacteriorhodopsin and maintain proton pumping ability. *J. Am. Chem. Soc.* 118:2552–53
154. Thorgeirsson TE, Xiao W, Brown LS, Needleman R, Lanyi JK, Shin YK. 1997. Opening of the cytoplasmic proton channel in bacteriorhodopsin. *J. Mol. Biol.* 273:951–57
155. Tittor J, Haupts U, Haupts C, Oesterheld D, Becker A, Bamberg E. 1997. Chloride and proton transport in bacteriorhodopsin mutant D85T: different modes of ion translocation in a retinal protein. *J. Mol. Biol.* 271:405–16
156. Tittor J, Oesterheld D. 1990. The quantum yield of bacteriorhodopsin. *FEBS Lett.* 263:269–73
- 156a. Tittor J, Schweiger U, Oesterheld D, Bamberg E. 1994. Inversion of proton translocation in bacteriorhodopsin mutants D85N, D85T and D85,96N. *Biophys. J.* 67:1682–90
157. Tittor J, Soell C, Oesterheld D, Butt HJ, Bamberg E. 1989. A defective proton pump, point mutated bacteriorhodopsin Asp96Asn, is fully reactivated by azide. *EMBO J.* 8:3477–82
158. Varo G, Lanyi JK. 1991. Effects of the crystalline structure of purple membrane on the kinetics and energetics of the bacteriorhodopsin photocycle. *Biochemistry* 30:7165–71
159. Varo G, Lanyi JK. 1991. Thermodynamics and energy coupling in the bacteriorhodopsin photocycle. *Biochemistry* 30:5016–22

160. Varo G, Lanyi JK. 1991. Kinetic and spectroscopic evidence for an irreversible step between deprotonation and reprotonation of the Schiff base in the bacteriorhodopsin photocycle. *Biochemistry* 30:5008–15
161. Varo G, Lanyi JK. 1991. Distortions in the photocycle of bacteriorhodopsin at moderate dehydration. *Biophys. J.* 59:313–22
162. Varo G, Lanyi JK. 1995. Effects of hydrostatic pressure on the kinetics reveal a volume increase during the bacteriorhodopsin photocycle. *Biochemistry* 34:12161–69
163. Vonck J. 1996. A three-dimensional difference map of the N-intermediate in the bacteriorhodopsin photocycle: part of the F helix tilts in the M to N transition. *Biochemistry* 35:5870–78
164. Vonck J, Han BG, Burkard F, Perkins GA, Glaeser RM. 1994. Two progressive substates of the M-intermediate can be identified in glucose-embedded, wild-type bacteriorhodopsin. *Biophys. J.* 67:1173–78
165. Weidlich O, Siebert F. 1993. Time-resolved step-scan FT-IR investigations of the transition from KL to L in the bacteriorhodopsin photocycle: identification of chromophore twist by assigning hydrogen-out-of-plane (HOOP) bending vibrations. *Appl. Spectrosc.* 47:1394–400
166. Weik M, Patzelt H, Zaccai G, Oesterhelt D. 1998. Localization of glycolipids in membranes by in vivo labeling and neutron diffraction. *Mol. Cell* 1:411–19
167. Weik M, Zaccai G, Dencher NA, Oesterhelt D, Hauss T. 1998. Structure and hydration of the M-state of the bacteriorhodopsin mutant D96N studied by neutron diffraction. *J. Mol. Biol.* 275:625–34
168. Xu D, Martin C, Schulten K. 1996. Molecular dynamics study of early picosecond events in the bacteriorhodopsin photocycle: dielectric response, vibrational cooling and the J, K intermediates. *Biophys. J.* 70:453–60
169. Yamazaki Y, Hatanaka M, Kandori H, Sasaki J, Karstens WJ, et al. 1995. Water structural changes at the proton uptake site (the Thr46-Asp96 domain) in the L intermediate in bacteriorhodopsin. *Biochemistry* 34:7088–93
170. Yamazaki Y, Sasaki J, Hatanaka M, Kandori H, Maeda A, et al. 1995. Interaction of tryptophan-182 with the retinal 9-methyl group in the L intermediate of bacteriorhodopsin. *Biochemistry* 34:577–82
171. Yamazaki Y, Tuzi S, Saito H, Kandori H, Needleman R, et al. 1996. Hydrogen bonds of water and C=O groups coordinate long-range structural changes in the L photointermediate of bacteriorhodopsin. *Biochemistry* 35:4063–68
172. Zhang NY, El-Sayed MA. 1993. The C-terminus and the Ca²⁺ low-affinity binding sites in bacteriorhodopsin. *Biochemistry* 32:14173–75
173. Zimanyi L, Cao Y, Chang M, Ni B, Needleman R, Lanyi JK. 1992. The two consecutive M substates in the photocycle of bacteriorhodopsin are affected specifically by the D85N and D96N residue replacements. *Photochem. Photobiol.* 56:1049–55